

Signatures of electronic ordering in transport in graphene flat bands

Archisman Panigrahi^{1,*} and Leonid Levitov¹

¹*Department of Physics, Massachusetts Institute of Technology, Cambridge, MA 02139, USA.*

(Dated: March 28, 2024)

Recently, a wide family of electronic orders was unveiled in graphene flat bands, such as spin- and valley-polarized phases as well as nematic momentum-polarized phases, stabilized by exchange interactions via a generalized Stoner mechanism. Momentum polarization involves orbital degrees of freedom and is therefore expected to impact resistivity in a way which is uniquely sensitive to the ordering type. Under pocket polarization, carrier distribution shifts in k space and samples the band mass in regions defined by the displaced momentum distribution. This makes transport coefficients sensitive to pocket polarization, resulting in the ohmic resistivity decreasing with temperature. In addition, it leads to current switching and hysteresis under strong E field. This behavior remains robust in the presence of electron-phonon scattering and is therefore expected to be generic.

Recent experiments reported on a cascade of strongly-correlated phases in moiré graphene multilayers [1–17] as well as their non-moiré counterparts [18–25], where the electronic properties can be tuned by altering the external displacement field (D) and the electron density (n). Moiré graphene hosts flat minibands with high density of states, where the effects of electronic interactions become significant [26–47]. Likewise, in non-moiré stacked graphene the displacement field opens up a gap and the resulting bands become remarkably flat near their extrema, giving rise to similar interaction-driven ordered phases [48–64]. To minimize the exchange energy, the electrons spontaneously break the combined $SU(4)$ symmetries in the spin-valley degrees of freedom, giving rise to valley-polarized and spin-polarized ferromagnetic orders [3–5, 7–11, 37–42, 50–52, 55].

Electronic ordering of a different kind can arise in non-moiré graphene multilayers when electrons partially fill the pockets induced by trigonal warping of carrier bands near the \mathbf{K} and \mathbf{K}' points. Such ‘carrier flocking’ in momentum space, driven by electron exchange interaction and described by Stoner-type instability, produces a nematic momentum-polarized order where only some of the pockets remain populated [23, 24, 61]. Upon temperature increasing, the ordering disappears through what is currently believed to be a continuous phase transition.

Several different techniques have been developed to probe electronic orders at low temperatures. Phase boundaries between different ordered phases can be probed by electronic compressibility measurements which capture the change in density of states at the Fermi surface, across the phase transition [19, 21, 23]. The low-temperature momentum-polarized, spin-polarized, and valley-polarized orders can be identified by quantum oscillations measurements [20], which reveal the spin/valley degeneracy and the Fermi surface geometry.

In comparison, the signatures of ordering in the temperature dependence of transport coefficients have received relatively little attention. The only transport sig-

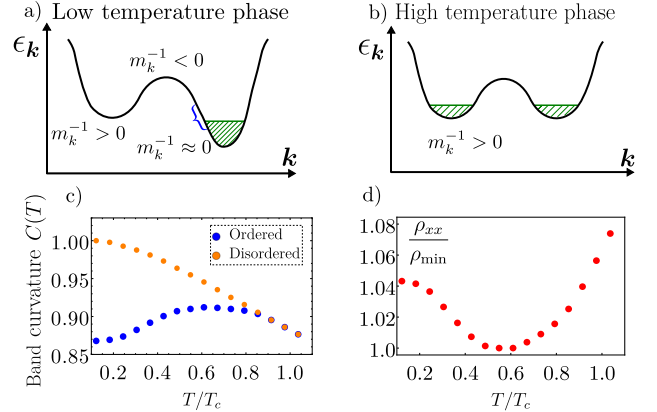


FIG. 1. (a), (b) Pocket-polarized and unpolarized states for a double-well 1D model, Eq.(11). Marked are regions in which the band curvature $m_k^{-1} = \partial^2 \epsilon_k / \partial k^2$ is positive, negative, and close to zero. The pocket-polarized carrier distribution shifts in k space and samples the band curvature, Eq.(1), in regions within the displaced momentum distribution. This makes transport coefficients sensitive to pocket polarization, resulting in ohmic resistance decreasing with temperature (see text). (c) Temperature dependence of the occupancy-weighted band curvature $C(T)$, Eq.(1), for the ordered states (blue) and the metastable disordered states (orange). (d) The resulting resistivity temperature dependence is nonmonotonic. Initially, it drops due to the increase in the band curvature of the ordered phase. At higher temperature the phonon scattering grows, and the resistivity increases linearly. Parameter values used are given in Sec.IV.

nature explored so far, which distinguishes symmetry-broken phases, was the anomalous Hall effect observed in the valley-polarized phase at low temperature [4, 22, 43]. In that, the \mathbf{K} and \mathbf{K}' valleys, which have opposite signs of Berry curvature, give rise to an anomalous Hall response resulting from broken time-reversal symmetry.

Motivated by recent findings [77], in this work we consider the longitudinal resistivity in the Ohmic regime (linear field-current response), and study the transport behavior in the non-Ohmic (nonlinear response) regime. Instead of the the Berry curvature, we focus on the band

* archi137@mit.edu

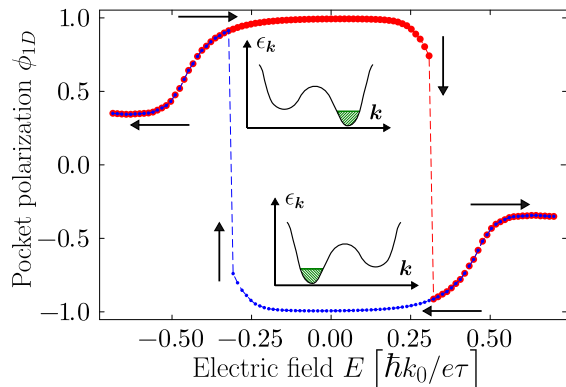


FIG. 2. Pocket polarization switching and history dependence of the dynamics under the action of an electric field for the model illustrated in Fig.1. As discussed in Sec.V, the initial state is the equilibrium state polarized in the right (left) pocket for the red (blue) curve. For each value of electric field E , we self-consistently determine the steady state, and plot the pocket polarization $\phi_{1D} = (n_R - n_L)/(n_R + n_L)$ against the (dimensionless) electric field. The right and left pocket-polarized steady states are pictured inside the hysteresis loop. For the right pocket-polarized initial state (red curve), for positive electric fields, the Fermi sea shifts to the $-\hat{k}_x$ direction, and the distribution switches to the left pocket at a finite electric field. No such switching occurs when the electric field is swept in the other direction. The opposite effect occurs for the left-pocket polarized initial state (blue curve). The black arrows show the direction of switching of the steady state when the electric field is swept.

dispersion and its dependence on the pocket-polarization ordering. As we will see, under pocket-polarization ordering, carrier distribution shifts in k space and samples the band curvature in regions defined by the displaced momentum distribution. This behavior makes transport coefficients sensitive to pocket polarization and leads to a unique signature of ordering—the negative temperature dependence of resistivity below the order-disorder transition. Namely, rising temperatures, despite increasing electronic disorder, drive the system into a more conducting state. This counterintuitive behavior originates from an interplay between exchange interactions that make carriers aggregate in Fermi pockets and thermal activation that excites carriers out of the Fermi pockets.

Furthermore, under the application of a strong electric field, the momentum-polarized phase can exhibit history dependence and switching of pocket polarization. This behavior is illustrated in Fig.2 which displays the results of a microscopic analysis developed in Sec.V. The resulting current switching may serve as an experimental test for discerning the proposed mechanism of negative temperature dependence of resistivity from alternative mechanisms.

I. TRANSPORT ANOMALIES DUE TO POCKET POLARIZATION ORDERING

As we will see, there is something unique and interesting about the metallic system in question, as it involves interplay of orbital degrees of freedom within flat bands, where a phase transition can significantly alter the geometry of the Fermi sea. Namely, the phase transition changes the band curvature $m_{k_i k_j}^{-1} = \partial^2 \varepsilon_{\mathbf{k}} / \partial k_i \partial k_j$ defined by the part of the band occupied by carriers,

$$C(T) = \left\langle \frac{\partial^2 \varepsilon_{\mathbf{k}}}{\partial k_x^2} \right\rangle_T = \frac{1}{n} \sum_{\mathbf{k}, \sigma} \frac{\partial^2 \varepsilon_{\mathbf{k}, \sigma}}{\partial k_x^2} f_{\mathbf{k}, \sigma}, \quad (1)$$

where $f_{\mathbf{k}, \sigma}$ is momentum distribution and $\varepsilon_{\mathbf{k}}$ is band dispersion which in itself depends, via exchange interaction, on $f_{\mathbf{k}, \sigma}$. (Here $n = \sum_{\mathbf{k}, \sigma} f_{\mathbf{k}, \sigma}$ is carrier density.) As illustrated in Fig.1(a) and (b), different parts of a two-pocket carrier band have curvature of opposite signs and, therefore, give opposite-sign contributions to $C(T)$.

As we will see, the changes in $C(T)$ driven by ordering translate into a characteristic T dependence of the resistivity. We will outline a mechanism through which the resistivity in the ordered phase at low-temperature can be higher than that of the disordered phase at a higher temperature. In other words, we argue that the resistivity can decrease with rising temperature, as the ordered phase melts. Negative temperature dependence, $d\rho/dT < 0$, stands in contrast with the sign of temperature dependence typically arising in clean metals due to carrier scattering by lattice vibrations. The low characteristic temperature at which it is expected to occur as well as the sign, make the negative $d\rho/dT$ a useful signature of pocket polarization ordering.

The mechanism leading to negative $d\rho/dT$ is illustrated in Fig.1. Using Boltzmann transport theory [66] the DC ohmic conductivity is given by the expression,

$$\sigma_{xx}(T) = \sum_{\mathbf{k}, \sigma} \frac{e^2 \tau(T)}{\hbar^2} \frac{\partial^2 \varepsilon_{\mathbf{k}, \sigma}}{\partial k_x^2} f_{\mathbf{k}, \sigma} = \frac{ne^2 \tau(T)}{\hbar^2} C(T), \quad (2)$$

where $f_{\mathbf{k}, \sigma}$ is the momentum distribution, $\sum_{\mathbf{k}}$ is a shorthand for $\int \frac{d^2 \mathbf{k}}{(2\pi)^2}$ and, for simplicity, the relaxation timescale τ is assumed to be momentum independent. Clearly, Eq.(2) implies that between two phases with comparable τ values, the one with greater average band curvature $C(T)$ will have a smaller resistivity.

The quantity $\varepsilon_{\mathbf{k}, \sigma}$ in Eq.(2) denotes the band dispersion modified by interactions, and $f_{\mathbf{k}, \sigma}$ is the Fermi function for this band dispersion. Under mean-field theory developed below, the pocket-asymmetric part of the momentum distribution $f_{\mathbf{k}, \sigma}$ plays the role of the order parameter describing pocket polarization. The energy $\varepsilon_{\mathbf{k}, \sigma}$ depends on $f_{\mathbf{k}, \sigma}$ and the non-interacting dispersion $\varepsilon_{\mathbf{k}}^0$ as

$$\varepsilon_{\mathbf{k}, \sigma} = \varepsilon_{\mathbf{k}}^0 - \sum_{\mathbf{k}' \neq \mathbf{k}} V(\mathbf{k} - \mathbf{k}') f_{\mathbf{k}', \sigma}, \quad (3)$$

where $f_{\mathbf{k},\sigma}$ is given by a Fermi distribution for the band dispersion modified by interactions,

$$f_{\mathbf{k},\sigma} = \frac{1}{e^{\beta(\varepsilon_{\mathbf{k},\sigma} - \mu)} + 1}, \quad (4)$$

and $V(\mathbf{k} - \mathbf{k}')$ represents the electronic interactions (see Sec.III). Eqs.(3) and (4), solved self-consistently, describe occupancy which becomes pocket-asymmetric at low temperature, as illustrated in Figs. 1 and 2. The occurrence of multiple fixed points for the self-consistent solution of these equations is a signature of a pocket symmetry breaking instability towards pocket polarization. Upon temperature increasing, the solution undergoes a transition to a disordered pocket-symmetric state.

We now discuss reasons for which the average occupancy-weighted band curvature, Eq.(1), can be lower in the low temperature phase than that in the corresponding high-temperature disordered phase, thus leading to resistivity decreasing with temperature. As an illustration, consider the momentum-polarized to unpolarized transition, focusing, for simplicity, on the pocket-polarized order in a single valley with a single spin species. Bilayer graphene hosts three pockets (or four pockets, at zero displacement field) induced by trigonal warping near its \mathbf{K}/\mathbf{K}' points. The regions in k -space where these pockets merge have a negative band curvature (hole-like), whereas the minima of the pockets have a positive band curvature. At low temperature, the ordered phase with a high enough electron density will be filled upto the neck of a single pocket (Fig.1(a)), and the band curvature of this pocket near the chemical potential will be much smaller than that near the pocket minima. As temperature is increased, the electrons will be thermally excited to (i) high-energy states within the same pocket, which either have a positive band curvature with smaller magnitude, or a curvature with negative sign, and, (ii) the low-energy states of the previously empty pocket, where the band curvature is positive and has relatively large magnitude. Clearly, there will be a competition between the two effects. When the electron density is high enough such that the chemical potential at low temperature is close to the minima of the empty pocket, the second effect wins due to the high density of states near this minima, and the occupation-averaged band curvature increases with temperature. Experimentally, such an effect may occur near the high density regions of the momentum-polarized phase in the $n - D$ phase diagram, D being the displacement field.

At low temperature (more specifically, below the Bloch-Grüneisen temperature [66–68]), phonons are not yet thermally activated, so the relaxation timescale $\tau(T)$ remains almost time-independent, and the resistivity will primarily depend on the band curvature. The resistivity decreases with rising temperature as the average band curvature increases due to gradual melting of the ordered phase. Eventually, the resistance will again linearly increase with temperature (i.e., the behavior of regular metals at room temperature) as the phonons become

thermally activated. In Sec. IV we establish this effect with two microscopic models that resemble the pockets in the bilayer graphene bandstructure (see Figs.1(d),4(c)).

It is interesting to note that this mechanism leads to temperature dependence of transport coefficients due to ordering which is considerably stronger than in the previously studied instances. An example that received considerable attention in the literature is the influence of spin-fluctuations on conductivity near a magnetic phase transition. A general argument for the contribution of this ordering to resistivity being weak was given by Fisher and Langer [65], who pointed out that the singular behavior of pair correlation functions at small k gives small contribution to the transport cross-section of carriers and concluded that the effect in the resistivity is weak. The weak T dependence predicted by this argument is in general in agreement with transport measurements in magnetic metals. In contrast, electronic ordering in graphene flat bands discussed here impacts carrier scattering at large angles, i.e. in a wide range of transferred momenta k . This makes resistivity sensitive to the ordering type, giving rise to the unique T dependence discussed below.

We also comment on other effects due to electron interactions that can potentially result in a negative temperature dependence of resistivity, $d\rho/dT < 0$. Some years ago, a similar effect in silicon MOSFETs has been studied and several mechanisms to explain it have been proposed. Those included the Coulomb scattering cross-section weakening at a higher temperature[71], an effect that leads to a decrease in the transport scattering rate. Other explanations focused on the effects due to the presence of charge traps and disorder[69, 70, 72].

Furthermore, in clean metals, carrier collisions were predicted a long time ago to result in hydrodynamic transport, wherein electrons undergoing two-body collisions behave as a viscous fluid[73]. Electron hydrodynamics was long believed to result in resistivity that decreases with temperature. Recently, however, it has been argued that the actual behavior is more nuanced[74]. Namely, correlated electron systems in a slowly varying disorder potential were predicted to show resistivity with a growing T dependence, an effect arising due to the interplay of heat conduction and thermoelectric effects. At the same time, transport in clean electron systems with sharp boundaries is expected to result in a negative temperature dependence of resistivity[75, 76]. The prediction of resistivity decreasing with temperature is supported by recent measurements [78, 79].

This behavior must therefore be accounted for in delimiting mechanisms leading to a negative T dependence in realistic systems. We note in that regard that there are several qualitative aspects of the pocket-polarization mechanism for negative temperature dependence of resistivity, $d\rho/dT < 0$, which make it distinct from the viscous electron flow mechanism. One is its lack of sensitivity to the cleanness of the system. This stands in contrast to electron hydrodynamics which requires the electron system to be ultra-clean. Another is that it is tied to temper-

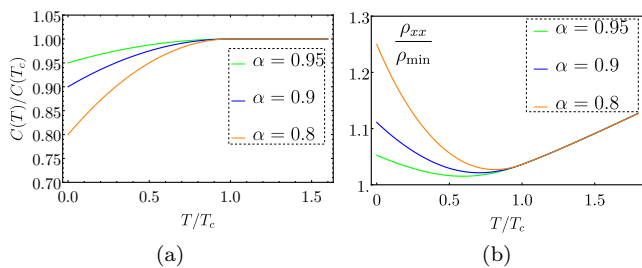


FIG. 3. (a) Band curvature of the ordered state $C(T)$ scaled by $C(T_c)$ in the phenomenological model, Eq.(5), for $\alpha = 0.8$ (orange curve), 0.9 (blue curve), and 0.95 (green curve), respectively. Here α denotes the ratio $C(T=0)/C(T=T_c)$ [see Eq.(5)] (b) Plots for resistivity (scaled by the minimum resistivity, which is of the order $\sim \hbar^2\gamma_0/ne^2C(T_c)$) of the phenomenological model for the values of α as in Fig.3(a). Parameter values used are given in Sec.II. The resistance initially decreases due to increase in average band curvature, and subsequently increases linearly due to phonon scattering.

ature at which the pocket polarization phase transition occurs. Lastly, as discussed below, pocket polarization order gives rise to a striking switching behavior of the nonlinear I - V dependence which coexists with the negative temperature dependence of resistivity. These properties will provide clear signatures of transport anomalies due to pocket polarization instability.

II. PHENOMENOLOGICAL PICTURE

Temperature dependence of transport coefficients near pocket-polarization ordering is governed by competition of two distinct effects. Firstly, pocket polarization results in carrier redistribution in k space. As temperature varies, carriers sample different parts of the band, producing temperature-dependent resistivity. Furthermore, because of exchange interactions, the band dispersion and band curvature become sensitive to pocket polarization, providing an additional source of temperature dependence. As our numerical results indicate, the combination of these effects can lead to a negative $d\rho/dT$. Secondly, electron-phonon interaction results in carrier scattering growing at temperatures above the Bloch-Grüneisen temperature, resulting in positive $d\rho/dT$ at high enough temperatures.

This behavior of the resistivity can be described phenomenologically as follows. At low temperature, the system is in the momentum-polarized ordered phase, which smoothly turns into the corresponding disordered phase through a continuous phase transition at temperature T_c . The conductivity of the system, given by Eq.(2), depends on the pocket polarization through the quantity $C(T)$, which is the band curvature weighted with the carrier momentum distribution. At very low temperature, the resistance is primarily affected by the band curvature,

as the phonons are not yet thermally activated, and the scattering rate is almost a constant. Above T_c , the resistance will primarily increase due to phonon scattering, and the curvature will play a minor role. Here, we use a phenomenological temperature dependence of band curvature and scattering rate to demonstrate that at low temperature, the resistance can decrease with rising temperature. Later, in Sec. IV, this behavior will be justified microscopically.

As we will see, the quantity $C(T)$ increases monotonically from $T = 0$ to $T = T_c$, where the ordered phase continuously turns into the disordered phase. This behavior can be modeled by a phenomenological dependence $C(T)$ which increases between $T = 0$ and $T = T_c$:

$$\frac{C(T)}{C(T_c)} = \begin{cases} 1 - (1 - \alpha) \left(1 - \frac{T}{T_c}\right)^2, & T < T_c \\ 1, & T \geq T_c, \end{cases} \quad (5)$$

with a suitable value $\alpha < 1$. Here $\alpha = C(T=0)/C(T_c)$. The specific form of Eq.(5) does not matter so long as $C(T)$ grows monotonically. The form of Eq.(5) is chosen so that it mimics the simulations of the microscopic models. For simplicity, we have set $C(T)/C(T_c) = 1$ above T_c , because there the temperature dependence of resistance is primarily determined by the phonon scattering. The exact temperature dependence of $C(T)$ obtained microscopically will be established below.

In addition to the band curvature, we must account for the temperature dependence of scattering by phonons and by disorder (defects or impurities),

$$\tau^{-1}(T) = \gamma_{\text{ph}}(T) + \gamma_{\text{dis}}(T). \quad (6)$$

At leading order, the disorder scattering rate γ_{dis} is a temperature-independent constant, γ_0 . The phonon scattering rate γ_{ph} is given by the Bloch-Grüneisen formula [66–68], which smoothly interpolates between a power law (quartic in 2D) below the Bloch-Grüneisen temperature $T_{\text{BG}} = \frac{2v_s\hbar k_F}{k_B}$, and a linear function above this temperature (here v_s is the speed of sound in the medium, and $\hbar k_F$ is the Fermi momentum). In this work, we approximate it with a simple phenomenological formula that interpolates between the two regimes, $\gamma_{\text{ph}}(T) = \gamma_1 \left(1 + (T/T_{\text{BG}})^4\right)^{1/4}$, giving

$$\gamma_{\text{ph}}(T) \approx \begin{cases} \frac{\gamma_1}{4} \left(\frac{T}{T_{\text{BG}}}\right)^4, & T \ll T_{\text{BG}} \\ \gamma_1 \frac{T}{T_{\text{BG}}}, & T \gg T_{\text{BG}}. \end{cases} \quad (7)$$

Below we set $\gamma_1 = 0.1\gamma_0$, so that the phonon scattering is relatively weak in the region of phase transition.

In bilayer graphene, the typical value of the Stoner-transition temperature T_c , and the Bloch-Grüneisen temperature T_{BG} are of the order $\sim 10K$. So, unless $T_{\text{BG}} \ll T_c$, the relaxation timescale will not significantly change in the course of the phase transition, and the resistivity

will decrease with increasing temperature. The variation of resistivity with temperature is plotted in Fig.3(b) for several values of α (we have chosen $T_{\text{BG}} = 0.8T_c$ throughout the paper). When $T_{\text{BG}} > T_c$, we find that the resistance continuously decreases with temperature until T_c , and it increases afterwards. When $T_{\text{BG}} \lesssim T_c$, the resistance decreases with temperature until it reaches T_{BG} . Afterwards, between T_{BG} and T_c , there will be a competition between the increasing curvature (which decreases resistance), and the increasing phononic scattering (which increases resistance). After reaching T_c , the resistance will increase with temperature. It is to be noted that system is in the metallic regime. The decrease in resistance occurs due to the decreased (average) curvature of the conduction band, which is very different from the phenomena observed in semiconductors, where the resistance decreases because the conduction band becomes thermally accessible at higher temperatures.

III. MICROSCOPIC FORMALISM

Here we introduce a microscopic approach that describes pocket-polarized order as a result of electron exchange interaction which leads to ‘carrier flocking’ in momentum space. Under a generalized Stoner mean field, the instability that leads to pocket asymmetry and pocket polarization is analogous to spin polarization instability in the Stoner magnetism. We will consider Hamiltonians of the form

$$H = \sum_{\mathbf{k},\sigma} \varepsilon_{\mathbf{k}}^0 c_{\mathbf{k},\sigma}^\dagger c_{\mathbf{k},\sigma} + \frac{1}{2} \sum_{\substack{\mathbf{k},\mathbf{k}' \\ \sigma,\sigma'}} V(\mathbf{q}) c_{\mathbf{k}-\mathbf{q},\sigma}^\dagger c_{\mathbf{k}'+\mathbf{q},\sigma'}^\dagger c_{\mathbf{k}',\sigma'} c_{\mathbf{k},\sigma}. \quad (8)$$

Under mean-field theory, we can write the interaction term as a combination of the so-called direct (Hartree) and exchange terms. As long as the average electron density is uniform (e.g. for Bloch waves), the Hartree term is just a constant which would not affect the electronic configurations.

In comparison, the exchange term favors carriers populating orbitals with equal spin and nearly equal momenta and can drive the instability towards carrier aggregation in momentum space. After dropping the (constant) Hartree term, we can write the mean-field free energy functional $F = E - TS$ as,

$$F[f_{\mathbf{k},\sigma}] = \sum_{\mathbf{k},\sigma} \varepsilon_{\mathbf{k}}^0 f_{\mathbf{k},\sigma} - \frac{1}{2} \sum_{\substack{\mathbf{k} \neq \mathbf{k}' \\ \sigma}} V(\mathbf{k} - \mathbf{k}') f_{\mathbf{k},\sigma} f_{\mathbf{k}',\sigma} + k_B T \sum_{\mathbf{k},\sigma} [f_{\mathbf{k},\sigma} \ln f_{\mathbf{k},\sigma} + (1 - f_{\mathbf{k},\sigma}) \ln(1 - f_{\mathbf{k},\sigma})], \quad (9)$$

where $f_{\mathbf{k},\sigma} = \langle c_{\mathbf{k},\sigma}^\dagger c_{\mathbf{k},\sigma} \rangle$ and the last term is the entropy contribution written in terms of the occupancy $f_{\mathbf{k},\sigma}$.

The functional $F[f_{\mathbf{k},\sigma}]$ defines a variational problem in the functional space $\{f_{\mathbf{k},\sigma}\}$ in which $f_{\mathbf{k},\sigma}$ are the varia-

tional parameters. To tackle this problem, it is convenient to work in the grand canonical ensemble by introducing the functional

$$\tilde{F}[f_{\mathbf{k},\sigma}] = F[f_{\mathbf{k},\sigma}] - \mu N, \quad (10)$$

where $N = \sum_{\mathbf{k},\sigma} f_{\mathbf{k},\sigma}$ and μ is a Lagrange multiplier that fixes the density N . To minimize the free energy, we consider the saddle-point conditions $\delta \tilde{F} / \delta f_{\mathbf{k},\sigma} = 0$, treating $f_{\mathbf{k},\sigma}$ as independent variables in the functional space. After some algebra we obtain coupled mean-field equations (3) and (4), which describe the minima of the functional \tilde{F} in the functional space of momentum distributions $f_{\mathbf{k},\sigma}$. We use iterations [82] to self-consistently solve these equations (for a single spin species) to determine the system ground state.

The unique aspect of the pocket-polarized states is spontaneous symmetry breaking. Normally, in the Landau Fermi-liquid framework, the problem of interacting fermions features a single ground state, representing a Fermi sea defined by the band dispersion $\varepsilon_{\mathbf{k},\sigma}$ renormalized by Fermi-liquid interactions but retaining the symmetry of the free-particle band. The self-consistent equations describing such ground states, derived from the Fermi-liquid theory, are essentially the same as our mean-field equations (3) and (4). At not-too-strong interactions $V(\mathbf{k} - \mathbf{k}')$ or at elevated temperature, these equations have a self-consistent solution representing a Fermi sea that has the point symmetry group identical to that of the free-particle band dispersion. While the point group for AB stacked bilayer graphene is D_{3d} , the band structure at each valley is invariant under C_3 rotations as well as by three σ_v mirror symmetries followed by time reversal.

At a larger interaction strength or at a lower temperature, the self-consistent equations acquire multiple solutions, including three solutions describing broken-symmetry pocket-polarized states forming an orbit of this generalized C_{3v} group and one solution describing a symmetry-unbroken unpolarized state. Conceivably, there are two scenarios for these states to emerge from a symmetry-unbroken state upon changing the interaction strength or varying temperature. One scenario is when the broken-symmetry solutions, when they first appear, have energies higher than the symmetry-unbroken state. Another scenario is when the broken-symmetry states, when they first appear, are the ground states, whereas the symmetry-unbroken state is a metastable state. In the first case, as the interaction strength increases or temperature decreases, the broken symmetry state emerges abruptly through a type-I transition, whereas in the second case it emerges continuously through a type-II transition. In our simulations, described below, the type-II transition scenario is observed upon varying temperature, whereas a type-I transition is seen upon varying carrier density or the interaction strength.

Determining fixed points the equations (3) and (4) corresponding to symmetry-unbroken and symmetry-broken states and disordered states was done by the method of

repeated iterations described below, which was found to converge reliably and rapidly enough. We found it more convenient to use the canonical ensemble picture with a fixed particle density rather than the grand-canonical ensemble framework. To numerically obtain a pocket-unpolarized (symmetry-unbroken) state (metastable below T_c) we initiate the iterations with identical carrier distributions in all the pockets. This is done by filling up energy states from the bottom of each pocket, until the total number of electrons reaches the desired value. To obtain the pocket-polarized ground state with a fixed number of electrons, we initiate the iterations with an out-of-equilibrium state with a particular pocket or two pockets being populated. Afterwards, we perform iterations by calculating the renormalized bandstructure with Eq.(3) and using it to find the new chemical potential, such that the sum of all the occupancies $f_{\mathbf{k},\sigma}$ (calculated using Eq.(4) with a given temperature) equals the desired number of electrons. Plugging these new $f_{\mathbf{k},\sigma}$ in Eq.(3), we keep repeating this procedure until a fixed point is reached. Above T_c , the equilibrium distribution becomes pocket-unpolarized (symmetry-unbroken), irrespective of whether the initial distribution of the iteration was pocket polarized or pocket-unpolarized.

IV. MODELING POCKET POLARIZATION IN 1D AND 2D SYSTEMS

Here we show how the behavior outlined in Sec.III emerges in simple models which resemble realistic bandstructures. We will start with a one-dimensional double-well band dispersion. This simple model captures the pocket-polarized order at low temperature, featuring an ordered phase that continuously turns into a disordered phase at some critical temperature T_c . At $T < T_c$, as temperature grows, the degree of pocket polarization diminishes. Simultaneously the occupancy-averaged band curvature $C(T)$ grows and ohmic resistivity exhibits the negative $d\rho/dT$ behavior pictured in Fig.1(d) and 4(c).

In this model, the two pockets of the non-interacting dispersion ε_k^0 are situated at some $\pm k_0$, where the band is relatively flat. The form of the interaction $V(\mathbf{k} - \mathbf{k}')$ is chosen to favor pocket polarization. For that, the inter-pocket interaction must be weaker than the intra-pocket interaction. These requirements are met by using the following bandstructure and interaction,

$$\varepsilon_k^0|_{1D} = E_0 \left(\frac{k^2}{k_0^2} - 1 \right)^2, \quad V(k-k') = V_0 e^{-\frac{(k-k')^2}{2q_0^2}}, \quad (11)$$

where the range of the gaussian interaction q_0 is chosen such that the interaction is negligibly small between different pockets, $q_0 \ll k_0$. For this model, by minimizing the free energy in Eq.(9), we verify that the system possesses an ordered pocket-polarized state which is thermodynamically stable below T_c . As T increases, a pocket-unpolarized state emerges at $T = T_c$ by a type-II

transition, where the order parameter vanishes. The order parameter describing pocket polarization can be chosen analogously to magnetization, but in terms of pocket populations rather than spins,

$$\phi_{1D} = \frac{n_R - n_L}{n_R + n_L}, \quad (12)$$

where n_L and n_R are the total electron numbers in the left and right pockets, respectively.

The numerical procedure through which an ordered state is obtained follows the description given in previous section. We initialize the system with a state which has a single pocket populated by all the electrons, and obtain the self-consistent solutions of Eq.(3) and Eq.(4) using iterations. This selfconsistent solution is polarized at low temperature, and becomes unpolarized (disordered) at temperatures above some T_c . We have set $q_0 = 0.2k_0$ and used a mesh of 1001 equidistant points between $k = -1.5k_0$ to $k = 1.5k_0$, populating the system with $N = 190$ electrons so that the low energy excitations fill-up states at the bottom of the empty pocket. Since the states away from the bottom of the pocket are unpopulated and are not thermally accessible at the temperatures we are working with, the boundary conditions of the lattice in momentum space do not affect our results, and we use open boundary conditions for convenience. For the simulation, we used dimensionless units $E_0 = 1$ and the value $V_0 = 0.004$ for the interaction strength.

For the values given above, the ordering temperature value was $T_c = 0.08$. This energy scale roughly corresponds to the distance between the Fermi level in a filled pocket and the bottom of the empty pocket. As discussed in Sec.I, there is a competition between thermal excitation to the high energy states of the filled pocket and the states at the bottom of the empty pocket in determining the temperature dependence of band curvature. To thermally excite majority of charge carriers to the bottom of the otherwise empty pocket, we set the density such that the equilibrium distribution at $T \approx 0$ resembles Fig.1(a), where the chemical potential is sufficiently close to the minima of the empty pocket. Then, as the temperature is increased, the empty pocket will be accessible to thermal excitation at low temperatures (without exciting very high energy states in the populated pocket), and the system will gradually go to the unpolarized phase. Throughout the process, the average curvature increases as the bottom of the initially unpopulated pocket becomes increasingly populated, and the resistance of the system decreases.

Now we describe how we numerically obtained the band curvature on a grid. We utilize a finite-difference method to estimate the second derivative of ε_k ,

$$\Delta_k^2 \varepsilon_k|_{1D} = \frac{\varepsilon_{k+\delta k} + \varepsilon_{k-\delta k} - 2\varepsilon_k}{(\delta k)^2}. \quad (13)$$

The average curvature of the ordered and the (metastable) disordered phases are plotted in Fig.1(c). Unlike the simplistic phenomenological model, where the

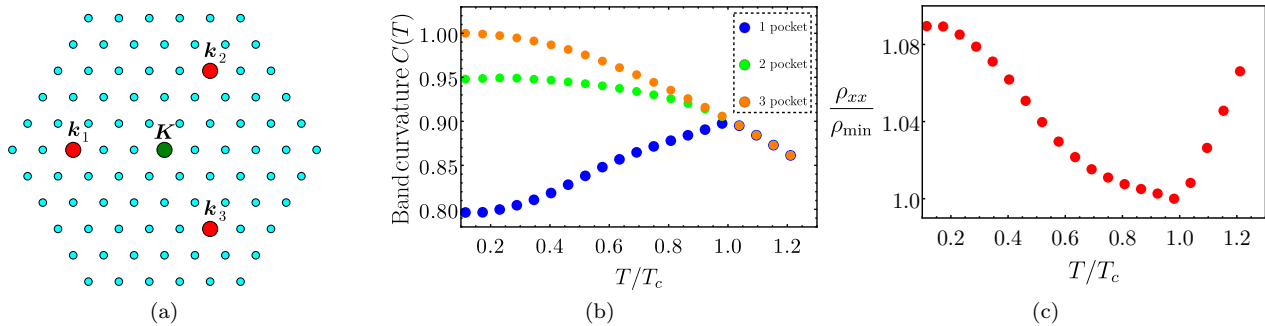


FIG. 4. (a) A triangular lattice in a hexagonal domain in momentum space, with 6 sites per side of hexagon, illustrating the configuration space used in the 2D model. The pockets are centered around the red points, with distance $k_0 = 3$ from the center (the \mathbf{K} point, shown in green) of the hexagon. In the actual simulation, we have used 24 sites per side of the hexagon, with $k_0 = 12$. (b) Variation of band curvature obtained numerically for the one-pocket (blue), two-pocket (green) and three-pocket/unpolarized (orange) states of the 2D model. They become identical near T_c , until which the curvature of the one-pocket state (ground state) increases as the temperature increases. Parameter values used are given in Sec. IV. (c) Temperature dependence of resistivity for the 1 pocket state. In this model, the resistivity increases very quickly after reaching T_c , because of the sharp change in the slope of the band curvature (blue curve in Fig.4(c)). It is really a very quick increase in slope rather than a non-analytic cusp.

curvature of the disordered phase was assumed to be a constant, here the curvature of the disordered phase decreases as temperature increases.

We use this microscopic model with Eqs. (2) and (6) to determine the resistivity vs. temperature dependence shown in Fig.1(d). Initially, the resistivity decreases because the average curvature of the ordered state increases as the system smoothly goes to the disordered state. Near T_c , the average curvature does not increase much, rather it begins to decrease because the system is almost disordered and the high energy states begin to be thermally populated, see Fig.1(c). Eventually, the phonon contribution becomes appreciable at $T > T_{BG}$, which causes an almost linear increase in resistivity for $T > T_c$.

In the second model, we consider a two-dimensional bandstructure with three pockets resembling the pockets induced by trigonal warping[64] near \mathbf{K}/\mathbf{K}' points in bilayer graphene. This model hosts one-pocket and two-pocket polarized phases at low temperature, which continuously turn into a disordered (unpolarized) phase at some T_c .

Here, the relevant order parameter \mathbf{D}_k is the (normalized) dipole moment of electrons in the momentum space, measured from the \mathbf{K} point,

$$\mathbf{D}_k = \frac{\sum_{\mathbf{k}} (\mathbf{k} - \mathbf{K}) f_{\mathbf{k}}}{\sum_{\mathbf{k}} k_0 f_{\mathbf{k}}}, \quad (14)$$

where k_0 is the distance of the center of a pocket from the \mathbf{K} point. The direction of this order parameter vector indicates which pockets have been polarized, and the magnitude identifies the nature of the polarization (i.e., one-pocket/two-pockets). By construction, the fully polarized one-pocket state has $|\mathbf{D}_k| = 1$, the two-pocket polarized state has $|\mathbf{D}_k| = 0.5$, and the order parameter is 0 for the unpolarized state. As we obtain the equi-

librium state at a particular temperature (iterating from a one-pocket or two-pocket polarized initial state), its dipole moment smoothly goes to zero, and that is how the critical temperature was estimated.

We use the following bandstructure and interaction

$$\begin{aligned} \varepsilon_{\mathbf{k}}^0|_{2D} &= -E_0 \sum_{i=1}^3 e^{-(\mathbf{k}-\mathbf{k}_i)^2/2q_1^2}, \\ V(\mathbf{k}-\mathbf{k}') &= V_0 e^{-(\mathbf{k}-\mathbf{k}')^2/2q_0^2}, \end{aligned} \quad (15)$$

where $\mathbf{k}_1 = k_0(-1, 0)$ and $\mathbf{k}_{2,3} = k_0\left(\frac{1}{2}, \pm\frac{\sqrt{3}}{2}\right)$ are the centers of the three pockets of radius q_1 , symmetrically placed on the vertices of an equilateral triangle.

This Hamiltonian was implemented on a triangular lattice in the momentum space (see Fig.4(a)), centered around the \mathbf{K} point (which is also the center of the $(\mathbf{k}_1, \mathbf{k}_2, \mathbf{k}_3)$ triangle). We use a triangular lattice so that all three pockets are equivalent and the discretized problem respects the trigonal symmetry. Similar to the previous model, we use open boundary condition, because the states at the boundary are never populated by electron in the range of electron density and temperature we consider. Parameter values used in our simulation were $E_0 = 1$, $V_0 = 0.01$, $k_0 = 12$, $q_1 = 4$, $q_0 = 6$, and we set $k_B = 1$. The results discussed below were obtained for a hexagonal domain with trigonal symmetry, with the total of 24 sites per side of the hexagon (see Fig.4(a)). The electron density was such that in the one-pocket polarized phase at $T \approx 0$, the chemical potential would be very close to the minima of the unoccupied pockets. The array within the hexagon was populated with $N = 82$ electrons so that this condition is satisfied. We find that as the temperature is increased while keeping the electron number fixed, the pocket-polarized

phase gradually melts into the disordered phase, and the resistivity decreases. In addition to the one-pocket polarized and pocket-unpolarized states, a two-pocket polarized state can also be considered. For this particular model, the ground state remains one-pocket polarized in low temperature, and the two-pocket polarized state (as well as the pocket-unpolarized state) is metastable. As temperature is increased, the one-pocket and two-pocket states gradually melt into the unpolarized state at a temperature T_c .

We evaluate the band curvature using a discrete lattice-laplacian implemented on the triangular lattice,

$$\Delta_{\mathbf{k}}^2 \varepsilon_{\mathbf{k}}|_{2\text{D}} = \frac{2}{3} \frac{\sum_{\langle \mathbf{k}' \rangle} \varepsilon_{\mathbf{k}'} - 6\varepsilon_{\mathbf{k}}}{(\delta k)^2}, \quad (16)$$

where $\sum_{\langle \mathbf{k}' \rangle}$ denotes the sum over the six nearest neighbors of \mathbf{k} , with δk the distance between nearest neighbors.

The resulting resistivity vs. temperature dependence is displayed in Fig.4(c). The resistivity steadily decreases until it reaches T_{BG} because the average curvature decrease in this regime, and the phonon scattering is negligible. Afterwards, between T_{BG} and T_c , there is a competition between the increasing curvature and the phonon scattering, and after reaching T_c , the resistance increases linearly.

V. SWITCHING INDUCED BY ELECTRIC FIELD

Upon the application of a spatially uniform and time-independent electric field, the whole Fermi sea begins to drift in the direction opposite to the electric field and the relaxation mechanism tries to restore the equilibrium distribution. The net result of this competition is that the Fermi sea is displaced from its equilibrium position in the steady state[66]. This can be modeled with the Boltzmann transport equation,

$$\frac{\partial f}{\partial t} + \frac{d\mathbf{r}}{dt} \cdot \frac{\partial f}{\partial \mathbf{r}} + \frac{d\mathbf{k}}{dt} \cdot \frac{\partial f}{\partial \mathbf{k}} = -\frac{f - f_0}{\tau}, \quad (17)$$

where f and f_0 are the non-equilibrium and the equilibrium distributions, respectively. In the steady state, $\frac{\partial f}{\partial t} = 0$, and $\frac{\partial f}{\partial \mathbf{r}} = 0$ due to spatial homogeneity. Also, $\frac{d\mathbf{k}}{dt} = -\frac{e\mathbf{E}}{\hbar}$ from the semiclassical equations of motion, where the charge of an electron is $-e$. Then, the equation reduces to

$$f(\mathbf{k}) - \frac{e\tau}{\hbar} \mathbf{E} \cdot \frac{\partial f(\mathbf{k})}{\partial \mathbf{k}} = f_0(\mathbf{k}). \quad (18)$$

This equation has a formal solution,

$$f(\mathbf{k}) = \frac{1}{1 - \frac{e\tau}{\hbar} \mathbf{E} \cdot \frac{\partial}{\partial \mathbf{k}}} \cdot f_0(\mathbf{k}). \quad (19)$$

To evaluate it, either the operator $\frac{1}{1 - \frac{e\tau}{\hbar} \mathbf{E} \cdot \frac{\partial}{\partial \mathbf{k}}}$ can be written as a Taylor series in $\mathbf{E} \cdot \frac{\partial}{\partial \mathbf{k}}$, or more formally, it can be evaluated using Fourier transforms, giving

$$f(\mathbf{k}) = \int_0^\infty ds e^{-s} f_0(\mathbf{k} + s e \mathbf{E} \tau / \hbar), \quad (20)$$

where s is an auxiliary integration variable.

At linear order in the electric field, the solution takes the form

$$f(\mathbf{k}) \approx f_0(\mathbf{k}) + \frac{e\tau}{\hbar} \mathbf{E} \cdot \frac{\partial f_0(\mathbf{k})}{\partial \mathbf{k}} \approx f_0(\mathbf{k} + e \mathbf{E} \tau / \hbar), \quad (21)$$

that is, the steady state Fermi distribution f will be a displaced version of the equilibrium Fermi distribution f_0 , as described above. If we take a pocket-polarized state, apply an electric field in the appropriate direction, and keep increasing its magnitude, at some point the displaced Fermi sea may abruptly switch, resulting in all the electrons shifting to another pocket. Since a finite electric field is required for the switching, the initial state cannot be restored by decreasing the magnitude of the electric field, or by the application of a small electric field in the opposite direction. Experimentally, such memory effects and history-dependent behavior in the transport properties may be observed by turning on a strong in-plane electric field, or by running high currents. These results, obtained here for a simple model, are expected to describe transport in a bilayer (or multi-layer) graphene or transition metal dichalcogenides (TMD) sample that hosts multiple Fermi pockets induced by trigonal warping[23, 24, 61]. The switching behavior, which is a consequence of pocket polarization assisted by an applied E field, may be used as an experimental probe for delineating pocket polarization from alternative mechanisms of negative $d\rho/dT$.

To model the switching effect, we modify the self-consistent equations (3) and (4) as follows. The exchange energy will depend on the field-induced steady-state distribution, modeled as the shifted equilibrium distribution. as discussed above. Namely, the coupled mean-field equations (3) and (4) must be replaced with the three equations

$$\varepsilon_{\mathbf{k},\sigma} = \varepsilon_{\mathbf{k}}^0 - \sum_{\mathbf{k}' \neq \mathbf{k}} V(\mathbf{k} - \mathbf{k}') f_{\mathbf{k}',\sigma}, \quad (22a)$$

$$f_{\mathbf{k},\sigma} = f_{\mathbf{k} + e \mathbf{E} \tau / \hbar, \sigma}^0, \quad f_{\mathbf{k},\sigma}^0 = \frac{1}{e^{\beta(\varepsilon_{\mathbf{k},\sigma} - \mu)} + 1}. \quad (22b)$$

To numerically solve these equations, we use the 1D model (Eq.(11)) with $E_0 = 1$, $k_0 = 1$, $V_0 = 0.01$, $q_0 = 0.2$, $k_B T / E_0 = 0.2$. We use the mesh of 2001 equidistant points between $k = -3k_0$ to $k = 3k_0$, and populating it with $N = 200$ electrons. We initiate the iterations with an equilibrium distribution polarized in the right (red curve in Fig.2) as well as the left pocket (blue curve in Fig.2), and in each case obtain a field-induced steady-state distribution.

To clarify the underlying physics, consider the evolution of the right pocket-polarized initial state. Under the application of a small positive electric field, the steady state distribution remains polarized at the same pocket, but as the electric field is increased, the distribution immediately switches to the left pocket, and the pocket polarization $\phi_{1D} = (n_R - n_L)/(n_R + n_L)$ discontinuously jumps from +1 to -1. The effect has been illustrated in Fig.2, where the switching occurs at $E \approx 0.32\hbar k_0/e\tau$ for the parameters mentioned in the previous paragraph. If we had swept the electric field in the opposite direction from the beginning (for the same right pocket-polarized initial state), then the steady state distribution would shift to the direction opposite to the left pocket. In this case, the system will not exhibit any switching behavior, but the pocket polarization ϕ_{1D} will gradually decrease in magnitude. Due to the displacement of the Fermi sea, the exchange energy at the minima of the filled pocket would be smaller compared to the initial state. Consequently, energy difference between the minima of the filled and the empty pockets would be smaller, and the initially empty pocket will gain some electrons due to thermal excitations. Therefore, the sign of ϕ_{1D} would remain the same, but it would decrease in magnitude, as observed in Fig.2. The analogous and opposite effect happens with the left pocket polarized initial state.

VI. DISCUSSION

The transport behavior discussed in this paper originates from pocket polarization. We restate the reasons for negative $d\rho/dT$ being a robust and generic property of the momentum-polarized order. At low temperatures, the electrons are predominantly scattered by impurities as the phonons are not yet thermally activated. Consequently, the resistivity of a metallic system is primarily determined by the average band curvature. Using microscopic models that mimic the pockets induced by trigonal warping in bilayer graphene and TMD, we demonstrated that the momentum-polarized ordered phase samples a greater number of states with relatively less curvature compared to its disordered counterpart, implying that the resistivity of the ordered phase will decrease with rising temperature, until the order undergoes melting. Subsequently, phonon scattering will reinstate the linear

dependence of resistivity on temperature, just like conventional metals at room temperature.

Another signature of momentum-polarized order is that transport in the ordered phase features a dependence on history. Namely, a particular momentum-polarized state can switch to a different momentum-polarized state when subjected to a strong electric field. This transition can give rise to hysteretic I - V characteristics that may be utilized to experimentally distinguish the mechanism of negative $d\rho/dT$ described above from other mechanisms.

A similar behavior in resistivity may be considered for the ‘valley-polarized’, and ‘spin-polarized’ ordered phases at very high carrier densities. However, for the scenario discussed above to be applicable, the bandstructure must be very different from standard bilayer graphene bandstructure near charge neutrality. Experimentally, the phases polarized in spin or valley, have only been stabilized at low electronic density (close to charge neutrality). Negative $d\rho/dT$ may be observed if the ordered state can be stabilized at a high enough electronic density so that it will sample an appreciable number of states with negative band curvature from the high energy necks linking the K or K' valleys, whereas the corresponding high-temperature state will sample a relatively greater number of states from the valley bottom, which has a positive band curvature. A bandstructure of this type is featured by biased antimonene, whose conduction band has several almost degenerate pockets [80, 81] which at a low temperature may host pocket-polarized phases. Further research is required to explore the resistive behavior of these systems. The longitudinal resistivity decreasing with temperature, combined with the switching behavior can serve as a transport signature to experimentally identify momentum-polarized ordered phases.

ACKNOWLEDGEMENTS

We are grateful to Andrea Young for sharing unpublished data and useful discussions, and to Dmitri Maslov for enlightening comments on the origin of a negative $d\rho/dT$ observed in silicon MOSFETs. This work was supported by the Science and Technology Center for Integrated Quantum Materials, National Science Foundation Grant No. DMR1231319.

-
- [1] Y. Cao, V. Fatemi, S. Fang, K. Watanabe, T. Taniguchi, E. Kaxiras, and P. Jarillo-Herrero, Unconventional superconductivity in magic-angle graphene superlattices. *Nature* 556, 43 (2018).
- [2] Y. Cao, V. Fatemi, A. Demir, S. Fang, S. L. Tomarken, J. Y. Luo, J. D. Sanchez-Yamagishi, K. Watanabe, T. Taniguchi, E. Kaxiras, R. C. Ashoori, and P. Jarillo-Herrero, Correlated insulator behaviour at half-filling in magic-angle graphene superlattices. *Nature* 556, 80

(2018).

- [3] A. L. Sharpe, E. J. Fox, A. W. Barnard, J. Finney, K. Watanabe, T. Taniguchi, M. A. Kastner, D. Goldhaber-Gordon, Emergent ferromagnetism near three-quarters filling in twisted bilayer graphene, *Science*, 365, 6453, 605-608 (2019)
- [4] M. Serlin, C. L. Tschirhart, H. Polshyn, Y. Zhang, J. Zhu, K. Watanabe, T. Taniguchi, L. Balents, A. F. Young. Intrinsic quantized anomalous Hall effect in a moiré het-

- erostructure. *Science*, 367, 6480 (2020)
- [5] C. L. Tschirhart, M. Serlin, H. Polshyn, A. Shragai, Z. Xia, J. Zhu, Y. Zhang, K. Watanabe, T. Taniguchi, M. E. Huber, A. F. Young, Imaging orbital ferromagnetism in a moiré Chern insulator, *Science*, 372, 6548, (1323-1327), (2021).
- [6] A. Kerelsky, L. McGilly, D. M. Kennes, L. Xian, M. Yankowitz, S. Chen, K. Watanabe, T. Taniguchi, J. Hone, C. Dean, A. Rubio, and A. N. Pasupathy, Maximized electron interactions at the magic angle in twisted bilayer graphene. *Nature* **572**, 95–100 (2019)
- [7] Y. Choi, J. Kemmer, Y. Peng, A. Thomson, H. Arora, R. Polski, Y. Zhang, H. Ren, J. Alicea, G. Refael, F. von Oppen, K. Watanabe, T. Taniguchi, and S. Nadj-Perge, Electronic correlations in twisted bilayer graphene near the magic angle. *Nat. Phys.* **15**, 1174-1180 (2019).
- [8] Y. Jiang, X. Lai, K. Watanabe, T. Taniguchi, K. Haule, J. Mao, and E. Y. Andrei, Charge order and broken rotational symmetry in magic-angle twisted bilayer graphene. *Nature* **573**, 91–95 (2019).
- [9] Y. Cao, D. Rodan-Legrain, J. M. Park, N. F. Q. Yuan, K. Watanabe, T. Taniguchi, R. M. Fernandes, L. Fu, and P. Jarillo-Herrero, Nematicity and competing orders in superconducting magic-angle graphene. *Science* 372, 264-271 (2021).
- [10] Y. Saito, F. Yang, J. Ge, X. Liu, T. Taniguchi, K. Watanabe, J. I. A. Li, E. Berg, and A. F. Young, Isospin Pomeranchuk effect in twisted bilayer graphene. *Nature* **592**, 220–224 (2021).
- [11] U. Zondiner, A. Rozen, D. Rodan-Legrain, Y. Cao, R. Queiroz, T. Taniguchi, K. Watanabe, Y. Oreg, F. von Oppen, A. Stern, E. Berg, P. Jarillo-Herrero, and S. Ilani . Cascade of phase transitions and Dirac revivals in magic-angle graphene. *Nature* 582, 203-208 (2020).
- [12] A. Rozen, J. M. Park, U. Zondiner, Y. Cao, D. Rodan-Legrain, T. Taniguchi, K. Watanabe, Y. Oreg, A. Stern, E. Berg, P. Jarillo-Herrero, and Shahal Ilani. Entropic evidence for a Pomeranchuk effect in magic-angle graphene. *Nature* 592, 214-219 (2021).
- [13] Y. Choi, H. Kim, Y. Peng, A. Thomson, C. Lewandowski, R. Polski, Y. Zhang, H. Singh Arora, K. Watanabe, T. Taniguchi, J. Alicea, and S. Nadj-Perge. Correlation-driven topological phases in magic-angle twisted bilayer graphene. *Nature* 589, 536-541 (2021).
- [14] A. T. Pierce, Y. Xie, J. M. Park, E. Khalaf, S. H. Lee, Y. Cao, D. E. Parker, P. R. Forrester, S. Chen, K. Watanabe, T. Taniguchi, A. Vishwanath, P. Jarillo-Herrero, A. Yacoby, Unconventional sequence of correlated Chern insulators in magic-angle twisted bilayer graphene. *Nature Physics*, 17(11), pp.1210-1215 (2021).
- [15] A. Fischer, Z. A. H. Goodwin, A. A. Mostofi, J. Lischner, D. M. Kennes, and L. Klebl . Unconventional superconductivity in magic-angle twisted trilayer graphene. *npj Quantum Materials* 7, 5 (2022)
- [16] N. J. Zhang, Jiang-Xiazi Lin, D. V. Chichinadze, Y. Wang, K. Watanabe, T. Taniguchi, L. Fu, J.I.A. Li. Angle-resolved transport nonreciprocity and spontaneous symmetry breaking in twisted trilayer graphene, [arXiv:2209.12964](https://arxiv.org/abs/2209.12964) (2022).
- [17] Z. Lu, T. Han, Y. Yao, A. P. Reddy, J. Yang, J. Seo, K. Watanabe, T. Taniguchi, L. Fu, L. Ju, Fractional Quantum Anomalous Hall Effect in a Graphene Moire Superlattice. [arXiv:2309.17436](https://arxiv.org/abs/2309.17436) (2023)
- [18] Y. Lee, S. Che, J. Velasco Jr., D. Tran, J. Baima, F. Mauri, M. Calandra, M. Bockrath, C. N. Lau, Gate Tunable Magnetism and Giant Magnetoresistance in ABC-stacked Few-Layer Graphene, [arXiv:1911.04450](https://arxiv.org/abs/1911.04450) (2019)
- [19] H. Zhou, T. Xie, A. Ghazaryan, T. Holder, J. R. Ehrets, E. M. Spanton, T. Taniguchi, K. Watanabe, E. Berg, M. Serbyn and A. F. Young, Half- and quarter-metals in rhombohedral trilayer graphene. *Nature* **598**, 429–433 (2021).
- [20] H. Zhou, L. Holleis, Y. Saito , L. Cohen , W. Huynh, C. L. Patterson, F. Yang, T. Taniguchi, K. Watanabe, and A. F. Young, Isospin magnetism and spin-polarized superconductivity in Bernal bilayer graphene. *Science* 375, 774-778 (2022).
- [21] S. C. de la Barrera, S. Aronson, Z. Zheng, K. Watanabe, T. Taniguchi, Q. Ma, P. Jarillo-Herrero, R. Ashoori, Cascade of isospin phase transitions in Bernal bilayer graphene at zero magnetic field. [arXiv:2110.13907](https://arxiv.org/abs/2110.13907) (2021)
- [22] H. Chen, A. Arora, J. C. W. Song and K. P. Loh, Gate-tunable anomalous Hall effect in Bernal tetralayer graphene. *Nat Commun* 14, 7925 (2023).
- [23] A. M. Seiler, F. R. Geisenhof, F. Winterer, K. Watanabe, T. Taniguchi, T. Xu, F. Zhang, R. T. Weitz, Quantum cascade of correlated phases in trigonally warped bilayer graphene. *Nature* 608, 298–302 (2022).
- [24] J-X Lin, Y. Wang, N J. Zhang, K. Watanabe, T. Taniguchi, L. Fu, J.I.A. Li, Spontaneous momentum polarization and diodicity in Bernal bilayer graphene, [arXiv:2302.04261](https://arxiv.org/abs/2302.04261)
- [25] Y. Zhang, R. Polski, A. Thomson, E. Lantagne-Hurtubise, C. Lewandowski, H. Zhou, K. Watanabe, T. Taniguchi, J. Alicea, and S. Nadj-Perge, Enhanced superconductivity in spin-orbit proximitized bilayer graphene. *Nature* **613**, 268–273 (2023)
- [26] J. M. B. Lopes dos Santos, N. M. R. Peres, and A. H. Castro Neto, Graphene Bilayer with a Twist: Electronic Structure, *Phys. Rev. Lett.* **99**, 256802 (2007)
- [27] E. J. Mele, Commensuration and interlayer coherence in twisted bilayer graphene, *Phys. Rev. B* **81**, 161405(R) (2010)
- [28] E. Suárez Morell, J. D. Correa, P. Vargas, M. Pacheco, and Z. Barticevic, Flat bands in slightly twisted bilayer graphene: Tight-binding calculations, *Phys. Rev. B* **82**, 121407 (R) (2010)
- [29] R. Bistritzer and A. H. MacDonald, Moiré bands in twisted double-layer graphene, *PNAS* 108 (30) 12233-12237 (2011)
- [30] F. Guinea and N. R. Walet, Electrostatic effects, band distortions, and superconductivity in twisted graphene bilayers, *PNAS* 115 (52) 13174-13179 (2018)
- [31] H. Isobe, N. F. Q. Yuan, and L. Fu, Unconventional Superconductivity and Density Waves in Twisted Bilayer Graphene, *Phys. Rev. X* **8**, 041041 (2018)
- [32] V. Kozii, H. Isobe, J. W. F. Venderbos, and L. Fu, Nematic superconductivity stabilized by density wave fluctuations: Possible application to twisted bilayer graphene, *Phys. Rev. B* **99**, 144507 (2019)
- [33] C. Xu and L. Balents, Topological Superconductivity in Twisted Multilayer Graphene, *Phys. Rev. Lett.* **121**, 087001 (2018)
- [34] Y.-P. Lin and R. M. Nandkishore, Chiral twist on the high-Tc phase diagram in moiré heterostructures, *Phys. Rev. B* **100**, 085136 (2019)

- [35] J. Kang and O. Vafek, Strong coupling phases of partially filled twisted bilayer graphene narrow bands, *Phys. Rev. Lett.* **122**, 246401 (2019)
- [36] M. Xie and A. H. MacDonald, Nature of the correlated insulator states in twisted bilayer graphene, *Phys. Rev. Lett.* **124**, 097601 (2020)
- [37] M. Ochi, M. Koshino, and K. Kuroki, Possible correlated insulating states in magic-angle twisted bilayer graphene under strongly competing interactions, *Phys. Rev. B* **98**, 081102(R) (2018)
- [38] Ferromagnetic Mott state in twisted graphene bilayers at the magic angle, K. Seo, V. N. Kotov, and B. Uchoa, *Phys. Rev. Lett.* **122**, 246402 (2019)
- [39] F. Wu and S. Das Sarma, Ferromagnetism and superconductivity in twisted double bilayer graphene, *Phys. Rev. B* **101**, 155149 (2020)
- [40] F. Wu and S. Das Sarma, Collective Excitations of Quantum Anomalous Hall Ferromagnets in Twisted Bilayer Graphene, *Phys. Rev. Lett.* **124**, 046403 (2020)
- [41] J. F. Dodaro, S. A. Kivelson, Y. Schattner, X. Q. Sun, and C. Wang, Phases of a phenomenological model of twisted bilayer graphene, *Phys. Rev. B* **98**, 075154 (2018)
- [42] S. Liu, E. Khalaf, J. Y. Lee, and A. Vishwanath, Nematic topological semimetal and insulator in magic angle bilayer graphene at charge neutrality, *Phys. Rev. Research* **3**, 013033 (2021).
- [43] N. Bultinck, S. Chatterjee, and M. P. Zaletel, Mechanism for Anomalous Hall Ferromagnetism in Twisted Bilayer Graphene. *Phys. Rev. Lett.* **124**, 166601 (2020)
- [44] Z. Dong, A. S. Patri, T. Senthil, Theory of fractional quantum anomalous Hall phases in pentalayer rhombohedral graphene moiré structures, [arXiv:2311.03445](https://arxiv.org/abs/2311.03445)
- [45] B. Zhou, H. Yang, Y.-H. Zhang, Fractional quantum anomalous Hall effects in rhombohedral multilayer graphene in the moiréless limit and in Coulomb imprinted superlattice, [arXiv:2311.04217](https://arxiv.org/abs/2311.04217)
- [46] J. Dong, T. Wang, T. Wang, T. Soejima, M. P. Zaletel, Ashvin Vishwanath, Daniel E. Parker, Anomalous Hall Crystals in Rhombohedral Multilayer Graphene I: Interaction-Driven Chern Bands and Fractional Quantum Hall States at Zero Magnetic Field, [arXiv:2311.05568](https://arxiv.org/abs/2311.05568)
- [47] Saisab Bhowmik, Arindam Ghosh, U. Chandni, Emergent phases in graphene flat bands, [arXiv:2309.08938](https://arxiv.org/abs/2309.08938) (2023)
- [48] E. V. Castro, N. M. R. Peres, T. Stauber, and N. A. P. Silva, Low-Density Ferromagnetism in Biased Bilayer Graphene, *Phys. Rev. Lett.* **100**, 186803 (2008)
- [49] E. V. Castro, K. S. Novoselov, S. V. Morozov, N. M. R. Peres, J. M. B. Lopes dos Santos, J. Nilsson, F. Guinea, A. K. Geim and A. H. Castro Neto, Electronic properties of a biased graphene bilayer, *J. Phys.: Condens. Matter* **22** 175503 (2010)
- [50] T. Stauber, E. V. Castro, N. A. P. Silva and N. M. R. Peres, First-order ferromagnetic phase transition in the low electronic density regime of a biased graphene bilayer. *J. Phys.: Condens. Matter* **20** 335207 (2008)
- [51] H. Min, G. Borghi, M. Polini, and A. H. MacDonald, Pseudospin magnetism in graphene, *Phys. Rev. B* **77**, 041407(R) (2008)
- [52] R. Nandkishore, L. Levitov, Flavor Symmetry and Competing Orders in Bilayer Graphene, [arXiv:1002.1966v1](https://arxiv.org/abs/1002.1966v1) (2010)
- [53] V. Cvetkovic, R. E. Throckmorton, O. Vafek, Electronic multicriticality in bilayer graphene, *Phys. Rev. B* **86**, 075467 (2012)
- [54] R. E. Throckmorton and S. Das Sarma, Quantum multicriticality in bilayer graphene with a tunable energy gap. *Phys. Rev. B* **90**, 205407 (2014)
- [55] J. Jung, M. Polini, and A. H. MacDonald, Persistent current states in bilayer graphene, *Phys. Rev. B* **91**, 155423 (2015)
- [56] Yang-Zhi Chou, Fengcheng Wu, Jay D. Sau, Sankar Das Sarma, Acoustic-phonon-mediated superconductivity in Bernal bilayer graphene, *Phys. Rev. B* **105**, L100503 (2022)
- [57] E. V. Gorbar, V. P. Gusynin, V. A. Miransky, and I. A. Shovkovy, Broken symmetry $\nu = 0$ quantum Hall states in bilayer graphene: Landau level mixing and dynamical screening, *Phys. Rev. B* **85**, 235460 (2012)
- [58] F. Zhang and A. H. MacDonald, Distinguishing Spontaneous Quantum Hall States in Bilayer Graphene, *Phys. Rev. Lett.* **108**, 186804 (2012)
- [59] M. Kharitonov, Antiferromagnetic state in bilayer graphene, *Phys. Rev. B* **86**, 195435 (2012)
- [60] A. Ghazaryan, T. Holder, M. Serbyn, and E. Berg, Unconventional Superconductivity in Systems with Annular Fermi Surfaces: Application to Rhombohedral Trilayer Graphene. *Phys. Rev. Lett.* **127**, 247001 (2021).
- [61] Z. Dong, M. Davydova, O. Ogunnaike, and L. Levitov, Isospin- and momentum-polarized orders in bilayer graphene, *Phys. Rev. B* **107**, 075108 (2023)
- [62] M. Koshino and E. McCann, Trigonal warping and Berry's phase $N\pi$ in ABC-stacked multilayer graphene, *Phys. Rev. B* **80**, 165409 (2009).
- [63] F. Zhang, B. Sahu, H. Min, and A. H. MacDonald, Band structure of ABC-stacked graphene trilayers, *Phys. Rev. B* **82**, 035409 (2010)
- [64] E. McCann and M. Koshino, The electronic properties of bilayer graphene, *Rep. Prog. Phys.* **76** 056503 (2013)
- [65] M. E. Fisher and J. S. Langer, Resistive Anomalies at Magnetic Critical Points, *Phys. Rev. Lett.* **20**, 665 (1968)
- [66] N. W. Ashcroft and N. D. Mermin, *Solid State Physics*. (1970), United States: Academic Press.
- [67] H. L. Stormer, L. N. Pfeiffer, K. W. Baldwin, and K. W. West, Observation of a Bloch-Grüneisen regime in two-dimensional electron transport, *Phys. Rev. B* **41**, 1278(R) (1990)
- [68] E. H. Hwang and S. Das Sarma, Acoustic phonon scattering limited carrier mobility in two-dimensional extrinsic graphene, *Phys. Rev. B* **77**, 115449 (2008)
- [69] Theory of Metal-Insulator Transitions in Gated Semiconductors, B.L. Altshuler and D.L. Maslov, *Phys. Rev. Lett.* **82**, 145 (1999).
- [70] Metal-insulator transition in 2D: resistance in the critical region, B.L. Altshuler, D.L. Maslov, and V.M. Pudalov, *Physica E* **9**, 209 (2001).
- [71] Temperature dependence of the conductivity for the two-dimensional electron gas: Analytical results for low temperatures, A. Gold and V.T. Dolgoplov, *Phys. Rev. B* **33**, 1076 (1986).
- [72] Interaction corrections at intermediate temperatures: Longitudinal conductivity and kinetic equation, Gábor Zala, B. N. Narozhny, and I. L. Aleiner, *Phys. Rev. B* **64**, 214204 (2001)
- [73] R. N. Gurzhi, Hydrodynamic Effects in Solids at Low Temperature, *Sov. Phys. Usp.* **11**, 255 (1968).

- [74] A. V. Andreev, S. A. Kivelson, and B. Spivak, Hydrodynamic Description of Transport in Strongly Correlated Electron Systems, *Phys. Rev. Lett.* **106**, 256804 (2011).
- [75] H. Guo, E. Ilseven, G. Falkovich, and L. Levitov, Higher-than-ballistic conduction of viscous electron flows, *Proc. Natl. Acad. Sci. U.S.A.* **114**, 3068 (2017).
- [76] P. Ledwith, H. Guo, A. Shtyov, L. Levitov Tomographic Dynamics and Scale-Dependent Viscosity in 2D Electron Systems, *Phys. Rev. Lett.* **123**, 116601 (2019).
- [77] A. F. Young, private communication.
- [78] R. Krishna Kumar, D. A. Bandurin, F. M. D. Pellegrino, Y. Cao, A. Principi, H. Guo, G. H. Auton, M. Ben Shalom, L. A. Ponomarenko, G. Falkovich, K. Watanabe, T. Taniguchi, I. V. Grigorieva, L. S. Levitov, M. Polini, and A. K. Geim, Superballistic flow of viscous electron fluid through graphene constrictions, *Nat. Phys.* **13**, 1182 (2017).
- [79] L. V. Ginzburg, C. Gold, M. P. Roosli, C. Reichl, M. Berl, W. Wegscheider, Th. Ihn, and K. Ensslin, Superballistic electron flow through a point contact in a Ga[Al]As heterostructure, *Phys. Rev. Research* **3**, 023033 (2021)
- [80] Atomically Thin Group V Elemental Films: Theoretical Investigations of Antimonene Allotropes Gaoxue Wang, Ravindra Pandey, and Shashi P. Karna *ACS Applied Materials & Interfaces* **2015** *7* (21), 11490-11496
- [81] Theory of 2D crystals: graphene and beyond. Rafael Roldán, Luca Chirolli, Elsa Prada, Jose Angel Silva-Guillén, Pablo San-Jose and Francisco Guinea. *Chem. Soc. Rev.*, 2017, **46**, 4387
- [82] The programs written in Julia for calculating the self-consistent solutions of Eq.(3) and Eq.(4), as well as Eq. (22) are available at <https://github.com/archisman-panigrahi/electronic-ordering-signature-resistance-codes>
-